

Assessing the influence of optically active constituents on the radiative heating of Laptev Sea surface waters

Mariana A. Soppa¹, Vasileios Pefanis¹, Sebastian Hellmann², Jens Hölemann¹, Markus A. Janout¹, Fedor Martynov³, Birgit Heim⁴, Vladimir Rozanov⁵, Svetlana Loza¹, Tilman Dinter¹ and Astrid Bracher^{1,5}

¹Alfred Wegener Institute, Helmholtz Centre for Polar and Marine Research, 27570 Bremerhaven, Germany

²ETH, 8092 Zurich, Switzerland

³Arctic and Antarctic Research Institute, 199397 St. Petersburg, Russia

⁴Alfred Wegener Institute, Helmholtz Centre for Polar and Marine Research, 14473 Potsdam, Germany

⁵Institute for Environmental Physics, University Bremen, 28359 Bremen, Germany

* Correspondence: msoppa@awi.de; Tel.: 49(471)4831-1869

1 Introduction

Studies have shown that the presence of CDOM and of SM in the Arctic waters results in an increased absorption of solar energy in the mixed layer (Pegau 2002, Hill 2008, Kutser 2010, Granskog et al. 2015, Kim et al. 2016); potentially contributing to sea ice melting. Here, we focus on the Laptev Sea shelf (Arctic Siberia), the region of the Arctic Ocean where the Lena River discharges - one of the largest river systems in the Arctic region and with the highest annual flux of dissolved organic carbon and silica to the Arctic Ocean (Stedmon et al. 2011, Holmes et al. 2012). In the Laptev Sea, the sea ice melting and break up of fast sea ice is coupled with the Lena River discharge (Bauch et al. 2013, Selyuzhenok et al. 2015). We hypothesize that the high concentrations of CDOM and SM of the Laptev Sea shelf waters highly absorb solar energy in the first few meters of the water column, trapping heat at surface and influencing sea ice melting and formation in the Lena delta.

To test the hypothesis, we combined efforts of satellite remote sensing, radiative transfer modeling and *in situ* sampling. In detail, we simulated the radiative heating in the water column and surface waters by using a coupled atmosphere-ocean radiative transfer model (RTM) and *in situ* measurements of a_{CDOM} (m^{-1}), suspended particulate matter (here after called total suspended matter - TSM, g/m^3) and chlorophyll concentration (Chla, mg/m^3) from the TRANSDRIFT XVII expedition carried out in September 2010. Moreover, we showed the potential of using satellite information together with RTM to investigate spatial variability of the radiative heating.

2 Methods

2.1 *In Situ* Data

The *in situ* dataset is composed of measurements of CDOM absorption spectra, SPM, Chla, temperature and salinity taken during August-September 2010 by the TRANSDRIFT-XVII (2010) expedition (Figure 1). Chla, temperature and salinity were

measured every 1 m, whereas the vertical resolution of a_{CDOM} and TSM varied among the stations. A detailed description of water sampling and analysis for the TRANSDRIFT XVII expedition can be found in Heim et al. (2014).

2.2 Radiative Transfer Model

The coupled atmosphere–ocean radiative transfer model (RTM) SCIATRAN release version 3.7.1 (Rozanov et al, 2002, 2014, 2017) was used for radiative heating simulations. SCIATRAN is freely available at <http://www.iup.physik.uni-bremen.de/sciatran> along with a detailed User’s Guide. The model spectral range covers from 0.18 to 2.4 μm and simulations were carried out from 0.3 to 0.9 μm in pseudo-spherical mode.

The atmospheric model of SCIATRAN includes thermal emission, absorption by several trace gases, Rayleigh scattering and scattering by aerosol and cloud particles. The ocean surface reflection properties are described by the bidirectional reflection function taking into account Fresnel effects and a wind roughened ocean-atmosphere using wind speed values derived from MERIS L1b data and extracted using Sentinel Application Platform (SNAP) software version 6.0. The solar spectrum is derived from MODerate spectral resolution atmospheric TRANsmittance algorithm and computer model (MODTRAN) 3.7 interpolated (1 nm) and convolved with a Gaussian full width at half maximum function. For the trace gases we used the spectral parameters and the climatologies provided by HITRAN 2012 database. The aerosol properties were selected as in Rozanov et al. (2017) and the aerosol optical thickness was set to 0.09 at 0.5 μm . Rotational Raman scattering and polarization effects were not included in the simulations.

The ocean model consists of biooptical models as described in Blum et al. (2012). Chlorophyll-a specific phytoplankton absorption coefficient is based on Prieur and Sathyendranath (1981) and Haltrin (2006), and mass-specific absorption spectrum of non-algal particles based on Örek et al. (2013). The pure water absorption (a_w) spectrum is a merged spectrum based on Smith (1981) for 200-300 nm with transition to Sogandares and Fry (1997) between 300-340 nm, Sogandares and Fry (1997) for 340-380 nm, Pope and Fry (1997) for 380-725 nm, Smith (1981) for 725-800 nm and Segelstein (1981) for 800-1150 nm. We further implemented a temperature and salinity correction following Röttgers et al. (2014). Particle scattering is based on Kopelevich (1983) with the concentrations of small and large particles determined following Haltrin (1999). No effects of vibrational Raman scattering and fluorescence by CDOM or Chla were included in the simulations.

2.3 Radiative heating simulations

As input parameters in the simulations, we used *in situ* profiles of a_{CDOM} spectrum, Chla, TSM, temperature, salinity and wind speed. To demonstrate the heating effect of large concentrations of the water constituents CDOM and TSM, simulations were performed for four stations of the TRANSDRIFT-XVII expedition. These stations presented the highest and lowest values of $a_{\text{CDOM}}(443)$ among all sampled stations with changing TSM

and Chla concentrations (Table 1).

To assess only the effect of the water constituents on the radiative heating, we simulated the spectrally integrated actinic flux (i.e. scalar irradiance, E_0 , W/m^2) for July 1 at 76°N, 126°E and for 24 solar zenith angles (representing hourly resolution). For the stations' simulations, also the MERIS imaging geometry information (solar zenith angle, satellite viewing angle and azimuth angle) for this specific location and day was considered.

From the actinic flux summed over the course of a day (KJ/m^2) we estimated the absorbed energy (E_{0abs}) at every vertical layer based on the provided depth grid (dz) as:

$$E_{0abs}(dz_i) = E_0(z_i + 1) - E_0(z_i) \quad (1)$$

with i ranging from zero to the maximum depth (z). Simulations were performed for different scenarios, including and excluding absorbers (Table 2). The difference in the absorbed energy (ΔE_{0abs}) was determined for example, by calculating the difference between E_{0abs} at S01 (highest a_{CDOM}) and at S40 (lowest a_{CDOM}). The ΔE_{0abs} for the upper 2 m can be translated in terms of radiant heat (RH, °C) as:

$$\Delta RH = \Delta E_{0abs} / \rho V c_p \quad (2)$$

where ρ is the density of seawater (kg/m^3) measured *in situ*, V is the volume of water (i.e. $2 m^3$) and c_p is the seawater specific heat ($4100 J/kg \text{ } ^\circ C$). Following the method described by Pegau (2002), we estimated the potential increase in the rate of sea ice melt (dH/dT , mm/h) caused by the presence of CDOM and TSM (considering that all E_{0abs} is converted to ice melt):

$$\Delta dH/dT = \Delta E_{0abs} / \rho L \quad (3)$$

where ΔE_{0abs} (KJ/m^2) is the difference in absorbed energy due to a_{CDOM} and TSM estimated from our simulations (as in equation 1 but given per hour), ρ is the density of sea ice ($900 kg/m^3$) and L is the latent heat of fusion of sea ice ($300 KJ/kg$).

2.4 Spatial distribution

The spatial analysis of radiative heating was simulated with satellite information of Chla, $a_{CDOM}(443)$, TSM and sea surface temperature (SST) for August 4, 2010; the least cloudy satellite image. More specifically, we used the C2RCC Laptev Sea Chla and C2RCC $a_{CDOM}(443)$ MERIS products after the evaluation of the satellite retrievals against *in situ* measurements. CDOM absorption spectra were derived from $a_{CDOM}(443)$ product using a spectral slope value of 0.018 (Matsuoka et al. 2014). TSM product was derived from the C2RCC algorithm. Temperature was estimated from SST using the Group for High Resolution Sea Surface Temperature (GHRSSST) Multi-scale Ultra-high Resolution (MUR) SST data [34] that combines information from microwave and infrared sensors and represents the temperature at 1 m depth. Salinity (S) was estimated empirically from satellite $a_{CDOM}(443)$ using a linear relationship derived from *in situ* measurements

TRANSDRIFT XXVII $S = 9.95 * a_{cdom}(440) + 32.49$ and assuming $a_{CDOM}(440) \approx a_{CDOM}(443)$. Constant light conditions were selected during simulations representing August 4, 2010, using an average solar zenith angle for the day at 74°N and 140°E. Considering that the shelf areas of the Laptev Sea are very shallow (Figure 1 and Table 1) and the average first optical depth was 2.6 m for the selected scene, the vertical distribution of Chla, $a_{CDOM}(443)$, TSM, salinity and temperature were set homogeneous with a constant bottom depth of 10 m.

3 Results and Discussion

3.1 Absorbed Energy and Radiant Heat

Profiles of E_{0abs} showed that in high CDOM and TSM regimes, the incident solar radiation was strongly absorbed in the first meter of the water column and almost fully attenuated in the upper five meters (Figure 2a). A closer look at S03 (Figure 2b), also a high a_{CDOM} station but with lower concentrations of TSM than S01, showed a turning point at 1.8 m; after this depth less energy was available and was absorbed in waters with the presence of CDOM. Similarly this was observed at S16 for simulations without CDOM or TSM, but at shallower depths (Figure 2c). As expected, in the marine-influenced waters of S40, where the concentration of CDOM, TSM and Chla were low, radiation penetrated deeper compared to the river-influenced stations and in turn, some of the heat could potentially be trapped below the pycnocline.

When a_{CDOM} was removed in the simulation at S03 (other absorbers were kept), there was 20% of difference in the E_{0abs} in the upper 2 m of the water column (Table 2). The highest $a_{CDOM}(443)$ station (S01) led to 15.8% more E_{0abs} in the surface layer relative to the station with lowest $a_{CDOM}(443)$ (S40). TSM presence also played a notable role on how much energy was absorbed at surface. But, even considering the highest TSM value measured in the field at S16, the concentration was not high enough to overcome the optical influence of CDOM on the E_{0abs} (Figure 8 c). By excluding TSM absorption and scattering effects, ΔE_{0abs} decreased by 4.6%, whereas the exclusion of a_{CDOM} led to a decrease of 5.9%.

The greater E_{0abs} by CDOM and TSM increased the RH. There was a temperature increase of 2.12°C/day in the top 2 m when a_{CDOM} was included in the simulations at S03 and a 0.55°C/day increase when TSM was included in the simulations at S16 (Table 2). A comparison between S01 and S40 showed an increased RH of 1.47°C/day. In addition, to directly compare our results with the study of Hill (2008) carried out in the Chukchi Sea, we also estimated the radiative heating at S16 for two hours exposure for summer (July 1, 2010) at solar noon. The combined effect of all absorbers at S16 led to 66% of increase in the surface heating and a 0.5°C increase in surface temperature. As expected, the temperature increase here observed was comparable but greater than the values reported by Hill (2008) (0.14°C), as the concentrations of CDOM and TSM in the Laptev Sea during TRANSDRIFT XVII expedition were significantly higher than in the Chukchi Sea.

The contribution of CDOM to sea ice melt was as high as 0.73 mm/h (S03, Table 2). In comparison, $\Delta H/dT$ caused by energy absorption due to TSM was lower, 0.19mm/h at S16, whereas the combined effect of CDOM and TSM led to a $\Delta H/dT$ of 1.2 mm/h. In waters under the influence of the Lena River plume, there was an increase of 0.5 mm/h in the ice melt rate relative to the marine-influenced waters. Given the bio-optical influence on the radiative heating in the Laptev Sea, a future with an amplified Arctic could have consequences to sea ice melt and thus, Arctic climate.

3.2 Radiative heating distribution

The spatial patterns of E_{0abs} and ΔRH confirm that the water constituents have significant influence on the radiative heating in the Laptev Sea surface waters (Figure 3). The largest E_{0abs} occurred over river influenced waters where also the ΔRH was enhanced. An analysis of the relationship between E_{0abs} , $a_{CDOM}(443)$, TSM and Chla revealed a more complex nature of relationships between the radiative heating and non-water absorbers that failed to be captured by point simulations (Figure 4). Although E_{0abs} increased with increasing $a_{CDOM}(443)$, the relationship became less definite when the concentration of TSM and Chla were higher than 10 g/m^3 and 3 mg/m^3 , respectively. As the concentration of TSM and Chla increase, also the size of these particles in the water increases causing higher scattering and light attenuation in the water. Evidence that should be supported by *in situ* observations in the future.

4 Conclusion

The effect of water constituents on the radiative heating of Laptev Sea shelf waters was investigated with the combined effort of satellite remote sensing, RT modeling and *in situ* sampling. The results show that the radiative heating of Laptev Sea surface waters is directly linked to the concentration of CDOM and TSM. The presence of the optically active constituents caused the ocean to absorb and deposit more energy in the upper 2 m of the water column. Likewise, waters where the amount of CDOM and TSM was higher presented an increased rate of sea ice melt compared to clearer waters. This implies that a detailed and realistic representation of optical properties of CDOM and TSM is necessary in Earth system models, especially on coastal waters and shelf regions. We also showed that the lack of *in situ* measurements can be compensated using satellite information together with RTM; this is especially important for remote and seasonally ice-covered regions as the Laptev Sea.

Acknowledgements: This study was funded by the German Science Foundation (DFG) Trans Regio SFB “Arctic Amplification TR 172” and Helmholtz Climate Initiative REKLIM (regional climate changes). Additional funding was provided by the Federal Ministry of Economics and Technology (BMWi) and the German Aerospace Centre grant number 50 EE 1620. The long-term Russian-German TRANSDRIFT expeditions in the Laptev Sea region were supported by the German Federal Ministry of Education and Research and the Russian Ministry of Education and Science. ESA is acknowledged for the MERIS satellite data and the SNAP software. The NASA EOSDIS Physical

Oceanography Distributed Active Archive Center (PO.DAAC) at the Jet Propulsion Laboratory, Pasadena, CA, is acknowledged for the SST data.

References

Bauch, D.; Hölemann, J.A.; Nikulina, A.; Wegner, C.; Janout, M.A.; Timokhov, L.A.; Kassens, H. Correlation of river water and local sea-ice melting on the Laptev Sea shelf (Siberian Arctic). *Journal of Geophysical Research: Oceans* 2013, 118, 550–561.

Blum, M.; Rozanov, V.; Burrows, J.; Bracher, A. Coupled ocean-atmosphere radiative transfer model in the framework of software package SCIATRAN: Selected comparisons to model and satellite data. *Advances in Space Research* 2012, 49, 1728–1742.

Granskog, M.A.; Pavlov, A.K.; Sagan, S.; Kowalczyk, P.; Raczowska, A.; Stedmon, C.A. Effect of sea-ice melt on inherent optical properties and vertical distribution of solar radiant heating in Arctic surface waters. *Journal of Geophysical Research: Oceans* 2015, 120, 7028–7039.

Heim, B.; Abramova, E.; Doerffer, R.; Günther, F.; Hölemann, J.A.; Kraberg, A.; Lantuit, H.; Loginova, A.; Martynov, F.; Overduin, P.P.; others. Ocean colour remote sensing in the southern Laptev Sea: evaluation and applications. *Biogeosciences*. 2014, 11, 4191–4210.

Haltrin, V.I. Chlorophyll-based model of seawater optical properties. *Applied Optics* 1999, 38, 6826–6832.

Haltrin, V. Absorption and scattering of light in natural waters. [in:] *Light scattering reviews single and multiple light scattering*, 2006.

Hill, V.J. Impacts of chromophoric dissolved organic material on surface ocean heating in the Chukchi Sea. *Journal of Geophysical Research: Oceans* 2008, 113.

Holmes, R.M.; McClelland, J.W.; Peterson, B.J.; Tank, S.E.; Bulygina, E.; Eglinton, T.I.; Gordeev, V.V.; Gurtovaya, T.Y.; Raymond, P.A.; Repeta, D.J.; others. Seasonal and annual fluxes of nutrients and organic matter from large rivers to the Arctic Ocean and surrounding seas. *Estuaries and Coasts* 2012, 35, 369–382.

Kim, G.E.; Gnanadesikan, A.; Pradal, M.A. Increased surface ocean heating by colored detrital matter (CDM) linked to greater northern hemisphere ice formation in the GFDL CM2Mc ESM. *Journal of Climate* 2016, 29, 9063–9076.

Kopelevich, O. Small-parameter model of optical properties of sea water. *Ocean Optics* 1983, 1, 208–234.

Kutser, T. Global change and remote sensing of CDOM in Arctic coastal waters. *OCEANS 2010 IEEE-Sydney*. IEEE, 2010, pp. 1–4.

Matsuoka, A.; Babin, M.; Doxaran, D.; Hooker, S.B.; Mitchell, B.G.; Bélanger, S.; Bricaud, A. A synthesis of light absorption properties of the Arctic Ocean: application to semianalytical estimates of dissolved organic carbon concentrations from space. *Biogeosciences* 2014, 11, 3131–3147. doi:10.5194/bg-11-3131-2014.

Naval Oceanographic Office, N.O.O. GHRSSST Level 4 K10_SST Global 1 meter Sea Surface Temperature Analysis. Ver. 1.0. PO.DAAC, CA, USA. <http://dx.doi.org/10.5067/GHK10-41N01>, 2018. Accessed: 2018-02-27.

Örek, H.; Doerffer, R.; Röttgers, R.; Boersma, M.; Wiltshire, K.H. Contribution to a bio-optical model for remote sensing of Lena River water. *Biogeosciences* 2013, 10, 7081.

Pegau, W.S. Inherent optical properties of the central Arctic surface waters. *Journal of Geophysical Research: Oceans* 2002, 107.

Pope, R.M.; Fry, E.S. Absorption spectrum (380–700 nm) of pure water. II. Integrating cavity measurements. *Applied optics* 1997, 36, 8710–8723.

Prieur, L.; Sathyendranath, S. An optical classification of coastal and oceanic waters based on the specific spectral absorption curves of phytoplankton pigments, dissolved organic matter, and other particulate materials 1. *Limnology and Oceanography* 1981, 26, 671–689.

Röttgers, R.; McKee, D.; Utschig, C. Temperature and salinity correction coefficients for light absorption by water in the visible to infrared spectral region. *Optics express* 2014, 22, 25093–25108.

Rozanov, V.V.; Buchwitz, M.; Eichmann, K.U.; de Beek, R.; Burrows, J.P. SCIATRAN - a new radiative transfer model for geophysical applications in the 240–2400 nm spectral region: the pseudo-spherical version. *Adv. Space Res.* 2002, 29, 1831–1835. doi:10.1016/S0273-1177(02)00095-9.

Rozanov, V.; Rozanov, A.; Kokhanovsky, A.; Burrows, J. Radiative transfer through terrestrial atmosphere and ocean: Software package SCIATRAN. *J. Quant. Spectr. Radiat. Transfer* 2014, 133, 13–71. doi:10.1016/j.jqsrt.2013.07.004.

Rozanov, V.; Dinter, T.; Rozanov, A.; Wolanin, A.; Bracher, A.; Burrows, J. Radiative transfer modeling through terrestrial atmosphere and ocean accounting for inelastic processes: Software package SCIATRAN. *Journal of Quantitative Spectroscopy and Radiative Transfer* 2017.

Segelstein, D.J. The complex refractive index of water. PhD thesis, University of Missouri–Kansas City, 1981.

Selyuzhenok, V.; Krumpfen, T.; Mahoney, A.; Janout, M.; Gerdes, R. Seasonal and interannual variability of fast ice extent in the southeastern Laptev Sea between 1999 and

2013. *Journal of Geophysical Research: Oceans* 2015, 120, 7791–7806. doi:10.1002/2015JC011135.

Smith, R.C.; Baker, K.S. Optical properties of the clearest natural waters (200–800 nm). *Applied optics* 1981, 20, 177–184.

Sogandares, F.M.; Fry, E.S. Absorption spectrum (340–640 nm) of pure water. I. Photothermal measurements. *Applied Optics* 1997, 36, 8699–8709.

Stedmon, C.; Amon, R.; Rinehart, A.; Walker, S. The supply and characteristics of colored dissolved organic matter (CDOM) in the Arctic Ocean: Pan Arctic trends and differences. *Marine Chemistry* 2011, 124, 108–118.

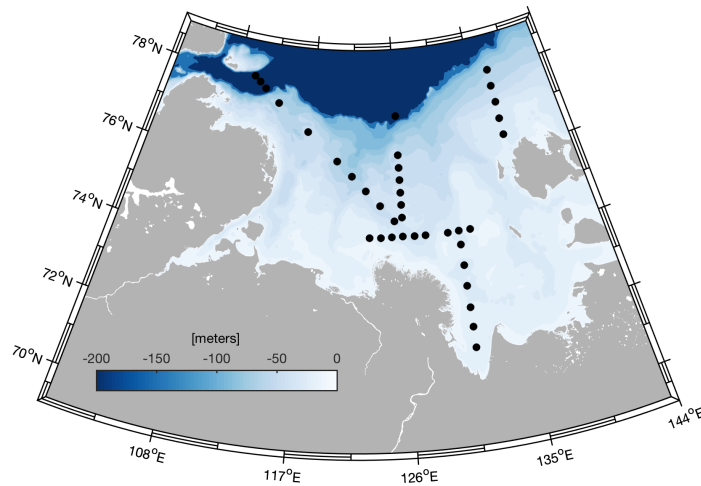


Figure 1. Study area and location of sampling stations of TRANSDRIFT-XVII expedition.

Table 1. Information about the selected stations for RTM simulation.

Station	Date	Longitude	Latitude	Bottom Depth	Temperature	Salinity	$a_{\text{CDOM}}(443)$	TSM	Chla	U
S01	09.09.10	131.00	71.5	14	7.66	7.80	1.77	1.60	2.03	4.5
S03	09.09.10	131.00	72.47	18	7.77	7.02	1.67	0.40	1.95	3.9
S16	13.09.10	123.99	74.33	17	4.10	19.05	1.08	7.20	0.84	9.1
S40	19.09.10	116.69	76.84	42	-0.19	28.04	0.20	0.17	0.40	3.4

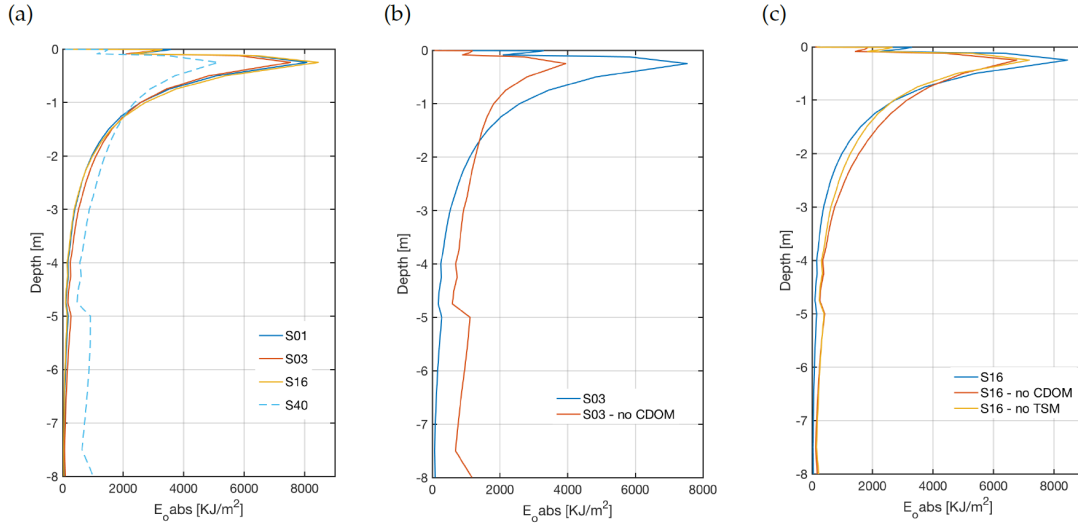


Figure 2. (a) Profiles of E_{0abs} including all absorbers. (b) Profiles of E_{0abs} at S03 including all absorbers (blue) and without CDOM (red). (c) Profiles of E_{0abs} at S16 including all absorbers (blue), without CDOM (red) and without TSM (orange).

Table 2. Absorbed energy difference (ΔE_{0abs} , KJ/m^2) and relative difference ($\% \Delta E_{0abs}$, KJ/m^2) at the top 2 m, absorbed energy difference in the subsurface layer ($\Delta E_{0abs\ 2-9\ m}$, KJ/m^2), radiant heating rate difference (ΔRH , $^{\circ}\text{C/day}$), ice melting rate difference ($\Delta \text{dH/dT}$, mm/h) for the selected scenarios.

Scenarios	ΔE_{0abs}	$\% \Delta E_{0abs}$	$\Delta E_{0abs\ 2-9\ m}$	ΔRH	$\Delta \text{dH/dT}$
S01 - S01 no CDOM	14170	15.8%	-9500	1.76	0.61
S03 - S03 no CDOM	17046	20.0%	-10232	2.12	0.73
S16 - S16 no TSM	4425	4.6%	-4095	0.55	0.19
S16 - S16 pure water	27967	38.0%	-3936	3.44	1.2
S01 - S40	11831	12.87%	-10928	1.47	0.5

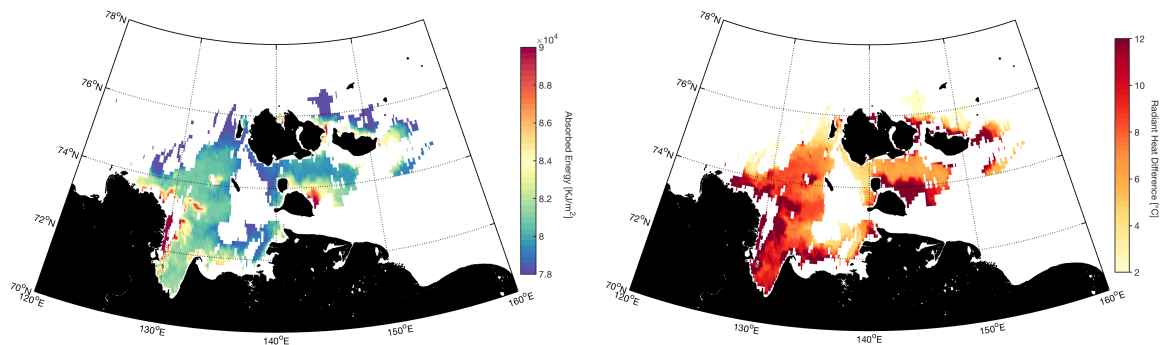


Figure 3. Spatial distribution of absorbed energy (left) and radiant heat difference (right) of the Laptev Sea surface waters.

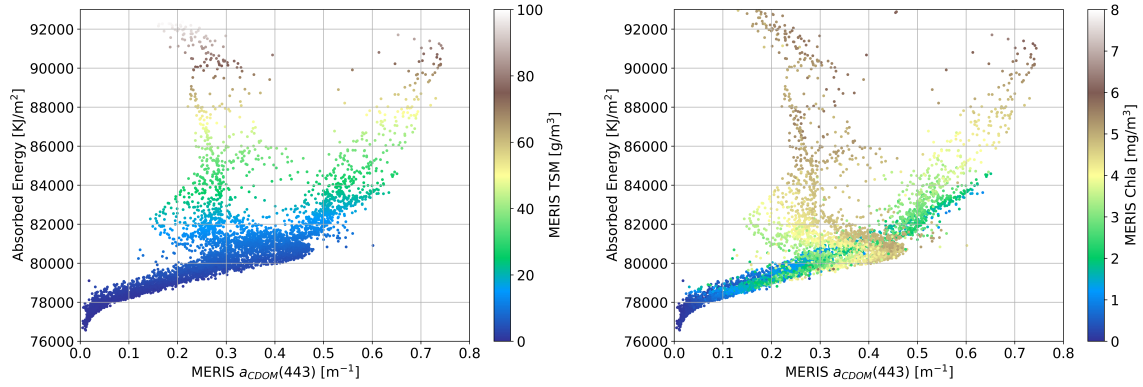


Figure 4. Scatterplot of E_{0abs} , $a_{CDOM}(443)$ and TSM (left) and scatterplot of E_{0abs} , $a_{CDOM}(443)$ and Chla (right).